Journal of Solid State Electrochemistry
https://doi.org/10.1007/s10008-024-05865-y

ORIGINAL PAPER

Li concentration change around Cu/LiPON interface measured by TOF-ERDA

Kyoshi Kurihara[1] · Shuri Nakamizo[2] · Satoshi Yamamoto[1] · Keisuke Yasuda[3] · Takuya Majima[2] · Takeshi Yajima[1] · Yasutoshi Iriyama[1]

Received: 28 January 2024 / Revised: 19 March 2024 / Accepted: 19 March 2024

Abstract
Lithium metal is a promising anode material for the development of advanced all-solid-state batteries (ASSBs) with high energy density. Among the various solid electrolytes, lithium phosphorus oxynitride glass electrolyte (LiPON) is notable for facilitating stable Li plating-stripping reactions in ASSBs employing Li metal. The aim of this study is to examine the Li/LiPON interface, with a specific emphasis on the reductive decomposition of LiPON near this interface. We employed time-of-flight elastic recoil detection analysis (TOF-ERDA) to assess changes in Li concentration around the Cu/LiPON interface immediately prior to the Li plating reaction. Our electrochemical measurements indicate that critical decomposition of LiPON occurs when the voltage at the Cu electrode is reduced to 0.1 V vs. Li/Li^+ at 25 °C, resulting in the in situ formation of Li_3P operating at 0.7 V vs. Li/Li^+ as an anode material. The TOF-ERDA findings reveal that this decomposition reaction results in a layer with partial decomposition (ranging from 5 to 25% on average) extending up to approximately 30 nm from the Cu/LiPON interface. This insight is vital for enhancing the design and performance of ASSBs.

Keywords All-solid-state battery · Li metal · LiPON · Interface · TOF-ERDA · Solid electrolyte interphase

Introduction

All-solid-state rechargeable lithium (Li) batteries (ASSBs) utilizing inorganic lithium-ion (Li^+) conductive solid electrolytes (SEs) are gathering significant interest as a next-generation battery. To enhance the energy density of ASSBs, employing a Li metal anode is crucial due to its substantially higher capacity (3860 mAh g^{-1}) compared to conventional graphite anodes (372 mAh g^{-1}). Among various SEs compatible with Li metal anodes, lithium phosphorus oxynitride glass electrolyte (LiPON) stands out as an especially promising material for stabilizing the Li/SE interface [1]. This is evidenced by the fact that thin-film-type ASSBs employing LiPON and Li metal anodes demonstrate stable charge–discharge cycles over 10,000 cycles without capacity degradation [2]. LiPON is typically prepared by RF magnetron sputtering and is conventionally formed only on an electrode layer [3]. However, recent developments in creating self-standing LiPON films have expanded its potential applications in advanced ASSBs [4].

Regarding the Li/LiPON interface in thin-film ASSBs, it is observed that Li plating-stripping reactions occur stably. Yet, advanced analyses indicate the formation of a reaction layer at this interface. Cheng et al. utilized Cryo-STEM analysis to investigate the Li/LiPON interface, revealing the generation of by-products like Li_2O, Li_3N, and Li_3P within an 80 nm thickness range from the interface [5]. Similarly, Sicolo et al. conducted XPS measurements on the LiPON surface before and after Li deposition, confirming the formation of a reaction layer immediately following Li layer deposition [6]. Theoretical calculations have suggested that LiPON reacts with Li metal, and the thermodynamical cathodic stability of LiPON is estimated to be 0.68 V vs. Li/Li^+ [7]. On the other hand, Schwietert et al. have reported that LiPON does not undergo reductive decomposition less

✉ Yasutoshi Iriyama
iriyama.yasutoshi@material.nagoya-u.ac.jp

[1] Department of Materials Design Innovation Engineering, Graduate School of Engineering, Nagoya University, Furo-Cho, Chikusa-Ku, Nagoya 464-8603, Japan

[2] Department of Nuclear Engineering, Kyoto University, Nishikyo-Ku, Kyoto 615-8540, Japan

[3] Graduate School of Life and Environmental Sciences, Kyoto Prefectural University, 1 Hangicho, Shimogamo, Sakyo-Ku, Kyoto 606-8522, Japan

Published online: 30 March 2024

than 0.68 V by taking a metastable state because an activation barrier for the decomposition can retard reductive decomposition [8]. Clarifying this interphase phenomenon is essential for the development of ASSBs with Li metal anodes.

In this work, we explored the potential of time-of-flight elastic recoil detection analysis (TOF-ERDA) for investigating Li concentration changes around the Cu/LiPON interface [9]. TOF-ERDA needs no sample pretreatment for the detection of Li, and then it can effectively observe Li concentration changes induced by electrochemical reactions around the interface. We will show that a decomposed region of LiPON forms around the interface within 30 nm thickness when maintained at 0.006 V vs. Li/Li^+ before the Li plating voltage at 0 V vs. Li/Li^+. Electrochemical analysis suggests one of the decomposed materials to be Li_3P [6]. These findings basically align with TEM–EELS data, underscoring the utility of TOF-ERDA in analyzing Li concentration changes around interfaces.

Experimental

Figure 1a shows a schematic cross-sectional image of the electrochemical cell to investigate Li concentration change around the Cu/LiPON interface. The base SE layer is mirror-polished Li^+ conductive $Li_{1+x}Al_xTi_{2-x}(PO_4)_3$ (LATP, LICGC AG-01: Ohara Inc. 150 µm in thickness). Both sides of the LATP were covered with LiPON film (thickness 2.5 µm) by RF magnetron sputtering (50 W, 3.2 Pa (N_2 atmosphere), deposition for 15 h, deposited at room temperature), and multilayered SE sheets (MLSE: LiPON/LATP/LiPON) were fabricated [10, 11]. The surface composition of LiPON was determined to be $Li_{2.0}PO_{2.6}N_{0.9}$ by X-ray photoelectron spectroscopy. Figure 1b shows a cross-sectional SEM image of the cell. As shown in Fig. 1b, LiPON film was uniformly formed on LATP. Although LATP is unstable against Li metal [10, 11], we have checked that this MLSE configuration realizes Li plating-stripping reactions without decomposing LATP [12, 13]. One side of the MLSE was covered with Cu film (30 nm in thickness, 10 mm × 10 mm in area) for Li concentration analysis, and the Cu film was prepared by RF magnetron sputtering (30 W, 1.5 Pa (Ar atmosphere), deposition for 5 min, deposited at room temperature without exposing the MLSE to the air). The opposite side assembled Li film (2–3 µm, 5 mm in diameter) as Li source, which was prepared by vacuum deposition equipped inside an Ar-filled glove box (dew point: < − 80 °C).

Electrochemical properties of the Li/MLSE/Cu cell were examined in an Ar-filled glove box (dew point less than − 80 °C) at 25 °C. All the voltages notated in this paper are referred to as Li/Li^+. Constant current and constant voltage (CCCV) measurements were carried out at 1 µA cm^{-2} in the range of 1.8–0.20 V or 1.8–0.006 V, and the cell voltage was maintained at each cutoff voltage for 60 min. Also, electrochemical impedance spectroscopy (200 kHz–30 mHz) was measured at 1.8 V and 0.006 V by applying an AC amplitude of 0.005 V before and after the CCCV measurements at 1.8–0.006 V.

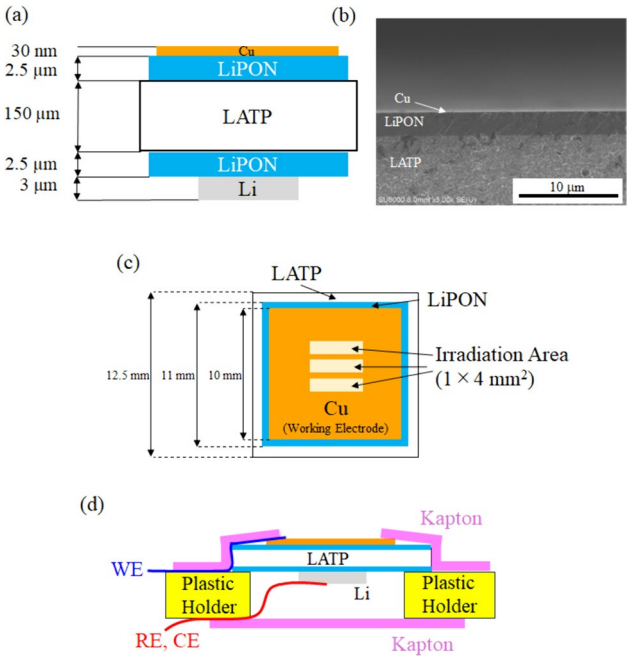

Fig. 1 **a** Schematic cross-sectional view of the Li/MLSE/Cu cell. **b** Cross-sectional SEM image of the cell. **c** Schematic top view of the cell, where TOF-ERDA measurements were carried at three different positions in the same at 1.8 V (AP), 0.006 V, and 1.8 V(DS). **d** Schematic image of the electrochemical holder for TOF-ERDA measurements

Figure 1c shows a schematic top-view image of the cell. This cell was mounted on plastic holder as shown in Fig. 1d. Here, the holder has a hole, and the cell was placed to cover the hole. Then, the cell edge was tightly sealed with Kapton adhesive tape so as to protect Li film during the attachment of the holder to the TOF-ERDA chamber in air. After the sample was placed in the chamber and connected to the electric cables, the chamber was evacuated to a base pressure of 10^{-5} Pa. CCCV measurements were carried out in the evacuated TOF-ERDA chamber at room temperature (~ 19 °C) in the range of 1.8–0.006 V under the same conditions as mentioned above. An ion beam (Cu^{5+}, 9 MeV) was irradiated only at each cutoff voltage to Cu film (working electrode) on the cell so that the total number of irradiated ions equaled 2.3×10^{13} cm^{-2}, where the beam current and irradiation time were 20 pA and 10 h, respectively. Among the various detected elements from the MLSE, this paper focuses on Li and P. The irradiation area was 1 mm × 4 mm (4 mm^2) as shown in Fig. 1c, and the radiation position was

changed at each measurement inside the same sample to eliminate ion-beam radiation damage.

Results and discussion

Figure 2a shows the charge–discharge curve of the Li/MLSE/Cu cell measured in a glove box, ranging from 1.8 to 0.2 V. Hereafter, we define charging as a reductive reaction and discharging as an oxidative reaction. The initial charging capacity at 1.8–0.2 V was 1.3×10^3 μC cm^{-2}, while the discharging capacity was 4.3×10^2 μC cm^{-2}. The capacity may be attributed to various sources such as the redox reaction of CuO [14, 15], formation of metastable state lithiated LiPON [8], and Cu-Li solid solution reaction [16], although their individual contributions remain unclear in this study. Figure 2b shows the charge–discharge curve of the cell at 1.8–0.006 V. During the first cycle, when the charging voltage was reduced to 0.006 V, a voltage plateau appeared around 0.1 V. The reductive current continued to flow while maintaining the voltage at 0.006 V, resulting in a final delivery of 8.2×10^3 μC cm^{-2}. At the discharging reaction, a new plateau emerged

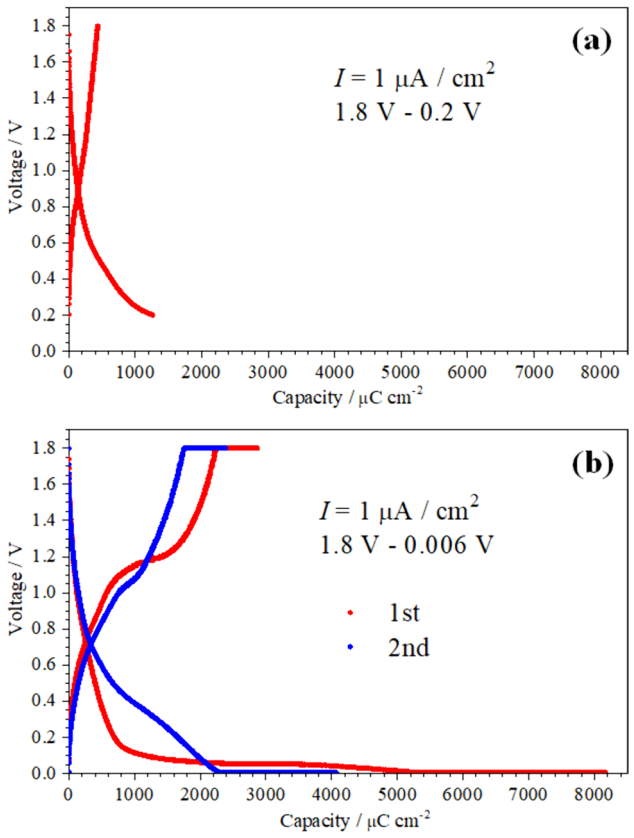

Fig. 2 CCCV curves of the Li/MLSE/Cu cells between **a** 1.8–0.2 V and **b** 1.8–0.006 V at 25 °C. Charge–discharge curves at first cycle is plotted as red, and the second one is as blue

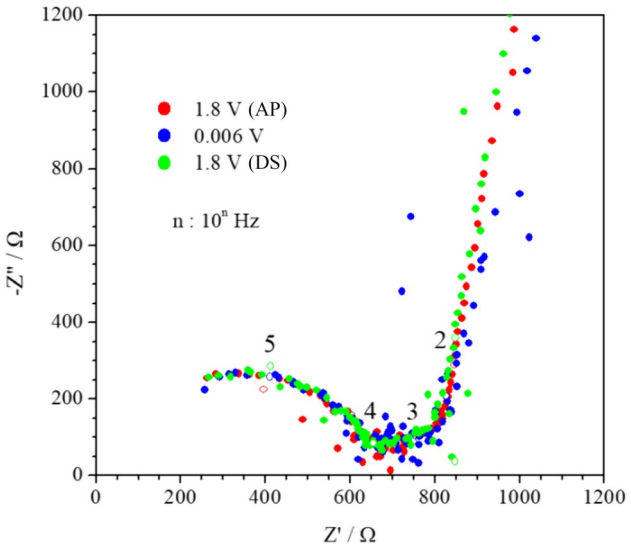

Fig. 3 Nyquist plots of the Li/MLSE/Cu cell at 1.8 V (AP, red), 0.006 V (blue), and 1.8 V (DS, green) measured at 25 °C

at 1.1 V with a total discharging capacity of 2.9×10^3 μC cm^{-2}. In the second charging reaction, the reductive reaction started at a higher voltage than the first charging reaction, with a plateau of around 0.5 V. The total capacity in the second charging reaction decreased to 4.1×10^3 μC cm^{-2}, which is 50% of the first charging reaction. On the other hand, the second discharging capacity was 2.4×10^3 μC cm^{-2}, maintaining 83% of the first discharging capacity, with a voltage plateau again at 1.0 V. These results suggest that LiPON undergoes critical decomposition around 0.1 V, which is below the theoretically expected cathodic potential window of 0.68 V. The Coulombic efficiency was 35% in the first cycle and increased to 59% in the second cycle. Additionally, the second discharging capacity decreased from 2.9×10^3 μC cm^{-2} to 2.4×10^3 μC cm^{-2}. These observations imply that the decomposed layer progressively grows with each charge–discharge cycle until a kinetically stable solid electrolyte interphase (SEI) layer forms, facilitating stable Li plating-stripping reactions [17]. When Li is deposited on the LiPON film, this reductive decomposition begins simultaneously from the Li/LiPON interface. [6]. The resultant by-product appears to undergo a redox reaction operating at 0.7 V in equilibrium. LiPON has been reported to yield Li_2O, Li_3N, and Li_3P as decomposed materials in both experimental analysis and theoretical calculations [6]. Li_3N is a Li^+-conductive solid electrolyte and oxidizes at 0.445 V [18]. Oxidation of Li_2O has been reported to occur around 3.0 V, and then Li_2O is not responsible for this capacity [19]. Li_3P is an anode material that operates at 0.7 V [20]. Therefore, the redox capacity observed in the first discharging reaction in Fig. 2b is likely due to Li_3P.

Figure 3 shows the Nyquist plots of the Li/MLSE/Cu cell measured in a glove box at 1.8 V as-prepared state (1.8 V(AP)), 0.006 V after the first charging reaction, and 1.8 V after the first discharging reaction (1.8 V(DS)). Each plot exhibits one semicircular arc in the high-frequency region ($> 10^4$ Hz), one smaller semicircular arc in the middle-frequency region (10^3–10^4 Hz), followed by a straight line to the real axis in the low-frequency region ($< 10^3$ Hz). As shown in Fig. 3, the Nyquist plots did not show any voltage dependencies and maintained a 1.8 V(AP) state even at 0.006 V and 1.8 V(DS). This indicates that reductive decomposition does not result in the formation of a highly resistive reaction layer for Li^+ conduction. Upon Li plating at the Cu/LiPON interface, another semicircular arc newly appears in the low-frequency region, and the spectrum settles on the real axis due to Li plating-stripping reactions [21, 22]. However, the Nyquist plots at 0.006 V did not show such spectrum change, suggesting that Li was not plated at the Cu/LiPON interface at this voltage. The decomposed material, Li_3P, is likely to be fully lithiated at 0.006 V, thus, charge transfer resistance does not appear at this voltage [20].

To investigate the changes in Li concentration around the Cu/LiPON interface before and after the critical decomposition of LiPON, TOF-ERDA measurements were conducted at 1.8 V(AP), 0.006 V, and 1.8 V(DS). The accuracy of estimating Li amounts by TOF-ERDA was validated in a model ASSB, $Fe_2(MoO_4)_3$/LATP/$LiCoO_2$ [23]. It was concluded that the Li concentration change in the $LiCoO_2$ electrode can be accurately measured by TOF-ERDA, with an accuracy of 10% [24]. Also, we measured the EIS spectrum of the Li/MLSE/Cu cell at 1.8 V(AP) after evacuation of the chamber (Supplemental Figure (SF.) 1) and checked that the EIS spectrum was almost consistent with that measured in the glove box. A slightly larger semicircular arc is probably because of a slightly lower temperature (~ 19℃) inside the chamber (Fig. 3).

Figure 4a shows the TOF spectra of Li in the Li/MLSE/Cu cell at 1.8 V(AP), 0.006 V, and 1.8 V(DS), where each data is plotted by a 5-point average, and then the *y*-axis is displayed as normalized intensity (NI). On these spectra, the horizontal axis indicates the channel number (Chn), which corresponds to the time-of-flight of Li particles recoiled from the cell and provides information on the kinetic energy of the recoiled Li particles. The vertical axis indicates the NI of recoiled Li, which is proportional to the Li concentration in the cell. The background NIs in Fig. 4 are lower than 10. The Li NIs decreased at higher channel numbers at 1.8 V(DS), but this trend was similarly observed for other elements, that is, P, O, N, and C (SF. 2). Thus, these trends are attributed to the slight differences in sample angle or beam position during the measurement, rather than a decrease in density or voltage-dependent diffusion of these elements [25]. The Cu surface and the Cu/LiPON

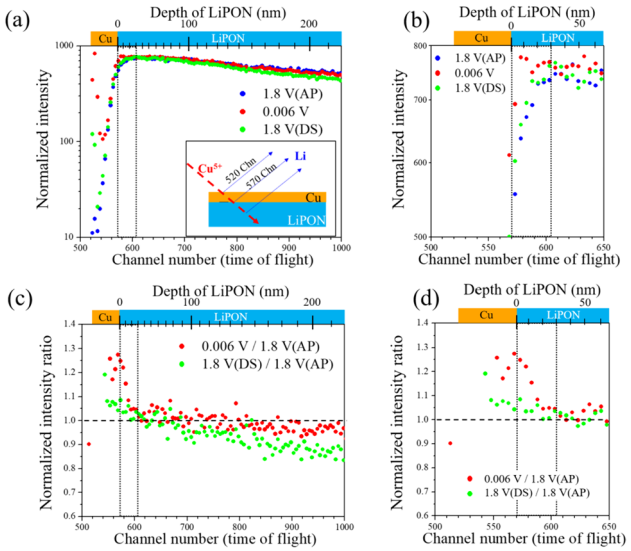

Fig. 4 **a** TOF spectra of Li from the Li/MLSE/Cu cell at 1.8 V(AP), 0.006 V, and 1.8 V (DS) at room temperature (~ 19 °C). The inset shows the schematic image of Cu^{5+} beam irradiation and recoiled Li detected at a given Chn. **b** Magnified TOF spectra around the Cu/LiPON interface. **c** Li NI ratio at 0.006 V and 1.8 V(DS) against 1.8 V (AP) at a given Chn. **d** Magnified NI ratio of Fig. 4**c**

interface positions were identified at 520 Chn and 570 Chn, respectively, using SIMNRA software [26]. The depth scale from the Cu/LiPON interface was evaluated using SIMNRA software as depicted on the upper horizontal axis of Fig. 4.

Figure 4b represents a magnified spectrum between 500 and 650 Chn from Fig. 4a, focusing on the voltage-dependent variable region surrounded by a dotted line in Fig. 4a. At 1.8 V(AP), there is a sharp increase in the Li NI around 570 Chn, indicating this position as the Cu/LiPON interface. Near the surface of Cu (520 Chn), the Li NI is about two orders of magnitude lower than around the Cu/LiPON interface in Fig. 1a, indicating an almost negligible presence of Li on the Cu surface in the 1.8 V (AP). At 0.006 V, the Li NI around the Cu/LiPON interface (570–610 Chn) slightly increases, indicating that Li accumulates in this Chn range. Furthermore, Li NIs are detected even around the Cu surface and inside the Cu film (520–570 Chn). It has been reported that Li forms a solid solution with Cu [16]. The higher Li NI near the Cu surface may result from side reactions between the Li-Cu alloy and residual gases in the chamber, similar to side reactions of electrochemically plated Li with the residual gases in SEM [12]. At 1.8 V(DS), the Li NI around the Cu/LiPON interface and inside the Cu film almost returns to the 1.8 V(AP) state. However, Li NIs are still observed near the Cu surface, probably due to unreacted Li remaining. The trend of Li NI beyond 570 Chn remains similar without voltage dependencies. The P NI distribution was also examined using TOF-ERDA as summarized in SF. 2a. The TOF spectra of P at 1.8 V are nearly overlapped, but the

TOF spectrum of P at 0.006 V shifts to higher Chn compared to the spectra at 1.8 V as shown in SF. 2a. Because P has a higher stopping power than Li [25], the presence of a Li-rich layer not only around the Cu/LiPON interface but also near the Cu surface, and Li-Cu alloy formation will effectively reduce the recoiled P energy, leading to the energy shift. However, apart from the Chn shift, the highest peak intensity of P NI at 0.006 V was almost consistent with that measured at 1.8 V(AP) and 1.8 V(DS), suggesting that the P concentration remains unchanged before and after the decomposition of LiPON, at least detectable levels by our TOF-ERDA measurements. This trend was also observed for O, N, and C with higher stopping power than Li (SF. 2b–d).

Figure 4c displays the Li NI ratio at 0.006 V and 1.8 V(DS) compared to 1.8 V(AP). At 0.006 V, the NI ratio increased to 1.25 around the Cu/LiPON interface and gradually decreased to 1.0 within a 30 nm thickness from the interface. This pattern aligns with TEM–EELS analysis, which shows that the decomposed region extends 76 nm from the interface, similar in scale to the Li-rich region formation detected by TOF-ERDA analysis. The composition of the LiPON used in this study, as estimated by XPS, was $Li_{2.0}PO_{2.6}N_{0.9}$. Based on previous reports, when LiPON fully decomposes into Li_3N, Li_2O, and Li_3P, the following decomposition reaction can be anticipated [6].

$Li_{2.0}PO_{2.6}N_{0.9} + 8.9\ Li^+ + 8.9e^- \rightarrow 2.6\ Li_2O + Li_3P + 0.9\ Li_3N$

When this reductive decomposition reaction occurs within a thickness of 1 nm, the Li NI is expected to increase by 5.5 times, resulting in a calculated charging capacity of approximately 2.2×10^3 μC cm^{-2}. Assuming that the total charging capacity measured in the TOF-ERDA chamber at 0.006 V (3.5×10^3 μC cm^{-2}, as shown in SF. 3) is consumed by this decomposition reaction, it suggests that LiPON undergoes reductive decomposition to a thickness of about 1.6 nm [6]. However, as observed in Fig. 4b, this decomposition appears to be distributed within a 30 nm range from the interface. The average Li NI ratio exceeding 1.0, observed within the 30 nm from the Cu/LiPON interface (between 570 and 605 Chn), is estimated to be 1.11, based on the area shown in Fig. 4d. This ratio corresponds to a partial decomposition of approximately 2.7% in this region. The charging capacity required for this partial decomposition is calculated to be 1.8×10^3 μC cm^{-2}. This value accounts for roughly 50% of the total charging capacity (3.5×10^3 μC cm^{-2}). The remained capacity will be utilized for reactions such as Cu-Li alloying as detected in Fig. 4a, and potentially for the charge–discharge reaction of metastable LiPON as well as Li insertion/extraction in CuO.

These findings indicate that partial decomposition of LiPON occurs over a relatively wide range in the depth direction from the Cu/LiPON interface. This decomposition reaction will occur very slowly at 25 ℃. In fact, once the charge–discharge reactions were carried out at 60 ℃, the plateau at 0.7 was observed during the initial charging reaction (SF. 4). Thus, this decomposition reaction will be kinetically retarded probably because of the presence of an activation barrier for the decomposition [8]. The decomposition region is distributed sparsely around the interface, and then Nyquist plots will not detect newly formed resistive sources even after the decomposition. However, this widespread decomposition likely determines the limit of LiPON thickness in thin-film ASSB. Although the ionic conductivity of LiPON has been successfully measured at thicknesses as low as 15 nm [27], thin-film-type ASSBs (e.g., Si/LiPON/LCO) exhibit rapid self-discharging when the LiPON thickness is below 100 nm [28]. Therefore, suppressing the growth of the decomposed area is a key factor in developing advanced ASSBs, especially using thinner layers of LiPON desirable for high-power ASSB.

Conclusion

The thermodynamical cathodic potential window of lithium phosphorus oxynitride glass electrolyte (LiPON) has been reported to be 0.68 V. However, our findings indicate that critical reductive decomposition of LiPON occurs at a lower potential of approximately 0.1 V at room temperature. This decomposition occurs in a region within 30 nm or less of the electrode interface at the first charging reaction at room temperature, characterized by partial decomposition (ranging from 5 to 25%, where 25% at Cu/LiPON interface and 5% at 30 nm from the interface) of LiPON. This trend was consistent with the past work investigated by TEM–EELS [5]. TOF-ERDA has proven to be an effective method for measuring these Li concentration changes, providing valuable insights into the stability and behavior of LiPON under varying electrochemical conditions.

Supplementary Information The online version contains supplementary material available at https://doi.org/10.1007/s10008-024-05865-y.

Funding Open Access funding provided by Nagoya University. This work was supported by JSPS KAKENHI "Interface IONICS" (JP19H05813, 20H05293, and 22H04617) and in part by JST GteX, JPMJGX23S2. The author (SY) would like to express special thanks to the "Interdisciplinary Frontier Next-Generation Researcher Program of Tokai Higher Education and Research System" for the financial support.

References

1. Chung K, Kim WS, Choi YK (2004) Lithium phosphorous oxynitride as a passive layer for anodes in lithium secondary batteries. J Electroanal Chem 566:263–267
2. Wang B, Bates JB, Hart FX, Sales BC, Zuhr RA, Robertson JD (1996) Characterization of thin-film rechargeable lithium batteries with lithium cobalt oxide cathodes. J Electrochem Soc 143:3203–3213
3. Dudney NJ, Neudecker BJ (2008) Solid state thin-film lithium battery systems. Curr Opin Solid State Mater Sci 4:479–482
4. Cheng D, Wynn T, Lu B, Marple M, Han B, Shimizu R, Sreenarayanan B, Bickel J, Hosemann P, Yang Y, Nguyen H, Li W, Zhu G, Zhang M, Meng YS (2023) A free-standing lithium phosphorus oxynitride thin film electrolyte promotes uniformly dense lithium metal deposition with no external pressure. Nat Nanotechnol 18:1448–1455
5. Cheng D, Wynn TA, Wang X, Wang S, Zhang M, Shimizu R, Bai S, Nguyen H, Fang C, Kim M, Li W, Lu B, Kim SJ, Meng YS (2020) Unveiling the stable nature of the solid electrolyte interphase between lithium metal and LiPON via cryogenic electron microscopy. Joule 4:2484–2500
6. Sicolo S, Fingerle M, Hausbrand R, Albe K (2017) Interfacial instability of amorphous LiPON against lithium: a combined Density Functional Theory and spectroscopic study. J Power Sources 354:124–133
7. Zhu Y, He X, Mo Y (2015) Origin of outstanding stability in the lithium solid electrolyte materials: insights from thermodynamic analyses based on first-principles calculations. ACS Appl Mater Interfaces 7:23685–23693
8. Schwietert TK, Vasileiadis A, Wagemaker M (2021) First-principles prediction of the electrochemical stability and reaction mechanisms of solid-state electrolytes. JACS Au 1:1488–1496
9. Yasuda K (2020) Time-of-flight ERDA for depth profiling of light elements. Quantum Beam Sci 4:40
10. Delmas C, Nadiri A (1988) The chemical short circuit method. An improvement in the intercalation-deintercalation techniques. Mater Res Bull 23:65–72
11. Amiki Y, Sagane F, Yamamoto K, Hirayama T, Sudoh M, Motoyama M, Iriyama Y (2013) Electrochemical properties of an all-solid-state lithium-ion battery with an in-situ formed electrode material grown from a lithium conductive glass ceramics sheet. J Power Sources 241:583–588
12. Sagane F, Shimokawa R, Sano H, Sakaebe H, Iriyama Y (2013) In-situ scanning electron microscopy observations of Li plating and stripping reactions at the lithium phosphorus oxynitride glass electrolyte/Cu interface. J Power Sources 225:245–250
13. Iwasaki S, Hamanaka T, Yamakawa T, West WC, Yamamoto K, Motoyama M, Hirayama T, Iriyama Y (2014) Preparation of thick-film $LiNi_{1/3}Co_{1/3}Mn_{1/3}O_2$ electrodes by aerosol deposition and its application to all-solid-state batteries. J Power Sources 272:1086–1090
14. Martin L, Martinez H, Poinot D, Pecquenard B, Le Cras F (2013) Comprehensive X-ray photoelectron spectroscopy study of the conversion reaction mechanism of CuO in lithiated thin film electrodes. J Phys Chem 117:4421–4430
15. Wang C, Higgins D, Wang F, Li D, Liu R, Xia G, Li N, Li Q, Xu H, Wu G (2014) Controlled synthesis of micro/nanostructured CuO anodes for lithium-ion batteries. Nano Energy 9:334–344
16. Mendelsohn MH, Gruen DM, Krauss AR (1986) Recent results on the preparation and properties of Li-containing Cu alloys. J Nucl Mater 141–143:184–187
17. Browning KL, Westover AS, Browning JF, Doucet M, Sacci RL, Veith GM (2023) In situ measurement of buried electrolyte–electrode interfaces for solid state batteries with nanometer level precision. ACS Energy Lett 8:1985–1991
18. Rabenau A (1982) Lithium nitride and related materials case study of the use of modern solid state research techniques. Solid State Ion 6:277–293
19. Abouimrane A, Cui Y, Chen Z, Belharouak I, Yahia HB, Wu H, Assary R, Curtiss LA, Amine K (2016) Enabling high energy density Li-ion batteries through Li_2O activation. Nano Energy 27:196–201
20. Mao E, Wang W, Wan M, Wang L, He X, Sun Y (2020) Confining ultrafine Li_3P nanoclusters in porous carbon for high-performance lithium-ion battery anode. Nano Res 13:1122–1126
21. Okita K, Ikeda K, Sano H, Iriyama Y, Sakaebe H (2011) Stabilizing lithium plating-stripping reaction between a lithium phosphorus oxynitride glass electrolyte and copper thin film by platinum insertion. J Power Sources 196:2135–2142
22. Iriyama Y, Kako T, Yada C, Abe T, Ogumi Z (2005) Charge transfer reaction at the lithium phosphorus oxynitride glass electrolyte/lithium cobalt oxide thin film interface. Solid State Ion 176:2371–2376
23. Kee Y, Suzuki Y, Ishigaki N, Motoyama M, Kimura Y, Amezawa K, Iriyama Y (2021) An appropriate reference and counter electrode in an all-solid-state battery using NASICON-structured solid electrolyte. Electrochem Commun 130:107108
24. Majima T, Ogura Y, Hasegawa C, Nakamizo S, Tsuchiya B, Amezawa K, Iriyama Y, Yasuda K (in preparation)
25. Alford TL, Feldman LC, Mayer JW (2007) Fundamentals of nanoscale film analysis. Springer, US, New York
26. Mayer M (1999) SIMNRA, a simulation program for the analysis of NRA, RBS and ERDA. AIP Conf Proc 475:541–544
27. Put B, Vereecken PM, Meersschaut J, Sepúlveda A, Stesmans A (2016) Electrical characterization of ultrathin RF-sputtered LiPON layers for nanoscale batteries. ACS Appl Mater Interfaces 8:7060–7069
28. Ruzmetov D, Oleshko VP, Haney PM, Lezec HJ, Karki K, Baloch KH, Agrawal AK, Davydov AV, Krylyuk S, Liu Y, Huang JY, Tanase M, Cumings J, Talin AA (2012) Electrolyte stability determines scaling limits for solid-state 3D Li ion batteries. Nano Lett 12:505–511